AMERICAN ACADEMY OF OPHTHALMOLOGY®

Geometrical Features of Subbasal Corneal Whorl-like Nerve Patterns in Dry Eye Disease

An In Vivo Confocal Microscopy Study

Ziqing Feng, MD, Kang Yu, MD, Yupei Chen, MS, Gengyuan Wang, MS, Yuqing Deng, MD, Wei Wang, MD, Ruiwen Xu, MD, Yimin Zhang, MD, Peng Xiao, PhD, Jin Yuan, MD, PhD

Purpose: To investigate the geometrical feature of the whorl-like corneal nerve in dry eye disease (DED) across different severity levels and subtypes and preliminarily explore its diagnostic ability.

Design: Cross-sectional study.

Participants: The study included 29 healthy subjects (51 eyes) and 62 DED patients (95 eyes).

Methods: All subjects underwent comprehensive ophthalmic examinations, dry eye tests, and in vivo confocal microscopy to visualize the whorl-like corneal nerve at the inferior whorl (IW) region and the straight nerve at the central cornea. The structure of the corneal nerve was extracted and characterized using the fractal dimension (CND_f), multifractal dimension (CND_0), tortuosity (CNTor), fiber length (CNFL), and numbers of branching points.

Main Outcome Measures: The characteristics of quantified whorl-like corneal nerve metrics in different groups of severity and subtype defined by symptoms and signs of DED.

Results: Compared with the healthy controls, the CND_f, CND_0, and CNFL of the IW decreased significantly as early as grade 1 DED ($P < 0.05$), whereas CNTor increased ($P < 0.05$). These parameters did not change significantly in the straight nerve. As the DED severity increased, CND_f and CNFL in the whorl-like nerve further decreased in grade 3 DED compared with grade 1. Significant nerve fiber loss was observed in aqueous-deficient DED compared with evaporative DED ($P < 0.05$). Whorl-like nerve metrics correlated with ocular discomfort, tear film break-up time, tear secretion, and corneal fluorescein staining, respectively ($P < 0.05$). Furthermore, merging parameters of whorl-like and linear nerve showed an area under the curve value of 0.910 in diagnosing DED.

Conclusions: Geometrical parameters of IW could potentially allow optimization of the staging of DED. Reliable and objective measurements for the whorl-like cornea nerve might facilitate patient stratification and diagnosis of DED.

Financial Disclosure(s): Proprietary or commercial disclosure may be found in the Footnotes and Disclosures at the end of this article. *Ophthalmology Science 2025;5:100669 © 2024 by the American Academy of Ophthalmology. This is an open access article under the CC BY-NC-ND license (http://creativecommons.org/licenses/by-nc-nd/4.0/).*

Dry eye disease (DED) is a growing global public health problem, with an estimated global prevalence of 5% to 35%, and China is one of the countries with a high incidence.[1,2] Dry eye disease impairs visual acuity and causes ocular discomfort, leading to changes in quality of life and financial burdens.[3] Therefore, early and accurate diagnosis for DED is crucial. Previous definitions emphasized the pathophysiological features of DED in terms of tear film instability, ocular surface inflammation, and damaged ocular surface epithelium.[4] However, neurosensory abnormalities are regarded as one of the key causes of DED and have been recently added to the updated definition of the Tear Film and Ocular Surface Society Dry Eye Workshop II in 2017. Chronic inflammation damages corneal nerves, impairing conduction and causing paresthesia, disrupting ocular surface homeostasis.[5]

As the body's most densely innervated tissue,[6] the cornea contains the subbasal nerve plexus (SBNP), assessed through in vivo confocal microscopy (IVCM).[7–10] Although it has been demonstrated that the corneal nerves are affected in DED in several studies, the opinions remain divided. Most studies have reported a decrease in nerve density in both Sjögren and non-Sjögren DED patients,[11,12] whereas others note no change or increased density in a specific subgroup.[13] These discrepancies arise from variations in DED stages and severity, resulting in different neurodegeneration/regeneration patterns and levels of inflammation.[5,14] Therefore, the changing trend of corneal nerves in different severities of dry eye remains to be determined.

Previous IVCM studies regarding DED have primarily focused on the assessment of straight nerve fiber bundles at

https://doi.org/10.1016/j.xops.2024.100669
ISSN 2666-9145/24

the SBNP.[11,15–17] Actually, nerve fibers converge to an area (known as inferior whorl [IW]) inferior and slightly nasal to the corneal apex, forming a distinct whorl-like pattern, which is a more distal part of the SBNP.[18] In particular, the SBNP at the IW region could serve as an ideal anatomical landmark for consistent scanning.[19] Intriguingly, recent studies verified that morphological metrics of the IW can potentially aide in early detection of diabetic neuropathy and small-fiber polyneuropathy in nervous system diseases.[20,21] However, little is known about alterations of IW structure in the DED setting. Therefore, an investigation into corneal nerves at the IW would further enhance the understanding of DED-induced corneal nerve injury.

Accurate extraction of nerve structures is crucial for quantitative analysis. Traditional methods for corneal nerve fiber segmentation and evaluation are time-consuming and semiautomated, warranting enhanced efficiency and accuracy.[22–24] With the development of deep learning algorithms, medical image segmentation technology has achieved breakthroughs, and convolutional neural networks have become a powerful tool for segmentation tasks and have been applied in various fields of ophthalmology.[25,26] Hence, it is reasonable to apply this technique to investigate the complex curvilinear structure of corneal nerves.

In this study, we aimed to explore the alterations of geometrical characteristics of whorl-like and straight corneal nerve in different severities and subtypes of DED, as well as their correlations with dry eye parameters.

Methods

Study Design and Participants

This cross-sectional study was conducted in Zhongshan Ophthalmic Center (Sun Yat-sen University, Guangzhou, China) between January 2021 and December 2022. This study was approved by the Medical Ethics Committee of Zhongshan Ophthalmic Center (2021KYPJ124) and was in accordance with the principles of the Declaration of Helsinki. Informed consent was obtained from all subjects before data collection.

Subjective symptoms of ocular discomfort were first assessed using a validated 12-item ocular surface disease index (OSDI) questionnaire with a scale of 0 to 100 points.[27] All participants then underwent comprehensive and standardized ophthalmic evaluations, including the following (listed in order): (1) assessment of the best-corrected visual acuity and intraocular pressure; (2) slit-lamp biomicroscopy examination; (3) noninvasive tear film break-up time (TBUT) measurement using the Keratograph 5M (Oculus); (4) corneal fluorescein staining (CFS) assessment by National Eye Institute grading scale[28]; (5) Schirmer test without anesthesia; (6) measurement of central corneal sensation using the Luneau 12/100-mm Cochet–Bonnet esthesiometer (Luneau; Prunay-LeGillon); and (7) IVCM using the Heidelberg Retinal Tomograph III Rostock Cornea Module (HRT3-RCM, Heidelberg Engineering).

The inclusion criteria were as follows: subjects over 18 years old, and the ability to understand the study consent and to cooperate with ocular examinations. Exclusion criteria included diabetes, neurological disorders, recent use of topical anti-inflammatory medications or optical soft contact lenses within 2 weeks before enrollment, eyelid malposition, active ocular allergy, previous diagnoses of Stevens–Johnson syndrome, mucous membrane pemphigoid, or infectious keratitis, and ocular surgery within the last 6 months. Participants with a known history of glaucoma in either eye were also excluded. Each eligible patient was thereafter assigned to either the DED group or the healthy control group as previously defined by Tear Film and Ocular Surface Society Dry Eye Workshop II criteria[29]: (1) an OSDI $\geq$13; (2) TBUT $<$10 seconds; or (3) $>$5 dots of CFS. The clinical severity of DED in each patient was assessed using a partially modified grading standard based on DEWS 2007,[4,30–32] in which a combination of DED symptom and clinical signs were used to classify disease severity. This classification scheme is objective and clinically applicable for grading DED currently. Because corneal nerve evaluations require high-quality IVCM images, eyes whose SBNP were difficult to identify were excluded. Patients were classified as having evaporative DED if their TBUT was $<$10 seconds and Schirmer test results exceeded 5 mm. On the other hand, if a patient exhibited both a low Schirmer test result ($<$5 mm) and a TBUT of $<$10 seconds, they were considered to have aqueous-deficient DED.[16,33]

In Vivo Confocal Microscopy Image Acquisition

All participants underwent IVCM examination. This process was performed by the same experienced examiner (Z.F.). The microscope enables a lateral spatial resolution of 0.5 μm and a depth resolution of 1 to 2 μm, generating coronal section images that cover a 400 × 400–μm area of cornea consisted of 384 × 384 pixels. To improve optical coupling, the objective lens of cornea module was covered by a disposable sterile cap (Tomocap, Heidelberg Engineering) coated with a layer of 0.2% carbomer eye gel. Both eyes of each subject received a drop of tetracaine hydrochloride for topical anesthesia. To recognize the central cornea, the images of subjects were captured in the primary gaze position, and red reflex from the laser of the IVCM was observed from a side camera to determine the corneal apex. The imaging depth was adjusted to capture the SBNP layer as clear as possible, typically at a depth of 50 to 80 μm. To locate the IW region, participants were instructed to gaze superonasally with their nonimaged eye at the external target. When the whorl-like structure was observed, placing the center of the whorl in the center of the field of view where possible. The image acquisition speed was 10 frames/second for SBNP in the central cornea and whorl-like zone.

Overlapping corneal nerve images and those containing stromal or epithelium layers (not in a single layer) or motion artifacts or folds were excluded by 2 masked independent investigators (K.Y. and R.X.) who had no access to the patient identity and clinical outcomes during IVCM image selection. The selected images were the best focused, completed and high contrast.[34] Finally, 3 representative images of SBNP in the central cornea and 1 in the whorl-like zone for each eye were selected for further quantified analysis.

Quantitative Assessment of Nerve Images

For nerve image segmentation and subsequent automatic calculation of morphologic metrics, a deep learning-based system for corneal nerve structure analysis which was developed and validated by our group.[35] Briefly, an encoder-decoder based semisupervized segmentation method was proposed for nerve segmentation and the segmented binary masks were skeletonized. An expert (J.Y.) clinician meticulously inspected each automatic segmentation result, and manual correction was carried out using NeuronJ plugin in ImageJ software (https://imagej.net/software/fiji/) if necessary. The following metrics were assessed: (1) corneal nerve fractal dimension (CND_f) was assessed by measuring the space-filling degree of a

fractal, reflecting the spatial availability of a complex shape[36,37]; (2) corneal nerve multifractal dimension (CND_0) was defined as the complex fractal structure divided into multiple regions, which is a more detailed evaluation of the complexity and inhomogeneity of a fractal and could reflect the density and complexity of complex curvilinear structure[37]; (3) corneal nerve tortuosity (CNTor) was based on the multiple segmentation algorithm to determine the degree of distortion[38,39]; (4) corneal nerve fiber length (CNFL) was defined as the total length of nerves per square millimeter (mm/mm^2); and (5) corneal nerve branching points (CNBPs, n/mm^2) was defined as the same point that is a start point for 1 nerve segment and an end point for another nerve segment. The final result of linear nerve was recorded as the mean values of 3 measurements. The final values of the above metrics were defined as the mean values obtained by the 2 masked investigators.

Statistical Analysis

All data were analyzed using SPSS 26.0 software. The distribution of variables was assessed using the Shapiro−Wilk test. Continuous variables were presented as mean ± standard deviation. Sex proportions were compared using the chi-square test. Age differences between groups were analyzed using Student *t* test. When both eyes of 1 participant were eligible, both eyes were included in the study. Cornea nerve metrics were compared between groups using generalized estimating equations (GEEs) to account for the correlation between fellow eyes of the same subject. Within GEE models, the statistical analysis of measurement data, which were consecutively acquired from both eyes of the same subject, was conducted as repeated measures. Pairwise comparisons were conducted using the least significant difference post hoc test within the GEE. Gender and age were included as covariates. Linear GEE models were employed to investigate the associations between OSDI, tear secretion, corneal sensation, TBUT, and geometric parameters of whorl-like nerves. A 2-sided critical *P* value of <0.05 was considered statistically significant. To explore the diagnostic value of corneal nerve geometrical features, the statistical analysis was conducted using R software (version 4.2.1). First, the least absolute shrinkage and selection operator was used for variables filtering and selection. Next, multivariate logistic regression was applied to construct combined predictive model for the diagnosis of DED. The discriminatory capacity of the model was evaluated by using the area under the receiver operating characteristic curve (AUC). Internal validation was performed by bootstrapping (1000 resampling). After that, the calibration of the model was assessed by the Hosmer−Lemeshow test.

Results

Demographic Data and Clinical Characteristics

A total of 146 eyes of 91 subjects were enrolled for the study, including 51 eyes of 29 healthy subjects (control group), and 95 eyes of 62 subjects with DED. Participants with DED were older than healthy controls ($P = 0.082$). There was no significant difference in sex distribution between the groups ($P = 0.075$). Compared with the healthy subjects, patients with DED had a higher OSDI, a shorter TBUT, a more severe National Eye Institute score, and lower Schirmer I test (all $P < 0.05$). However, there was no difference in central and peripheral corneal sensitivity between 2 groups. Detailed demographics and clinical data are summarized in Table 1. Table 2 represents the ocular surface characteristic of patients with DED of varying severity based on DEWS classification. Patients with DED had higher OSDI score and CFS with increasing sequence severity ($P < 0.001$). Tear film break-up times in grade 2 and grade 3 were lower than grade 1 ($P < 0.001$). The Schirmer I test in grade 3 was lower than grade 1 and grade 2 ($P < 0.001$).

Multiparametric Changes of Corneal Nerve in DED Patients

Figure 1 and Table 3 present geometric parameters of the whorl-like nerve for different levels of DED severity, after adjustment for the eye examined, gender, and age by GEE. The CND_f, CND_0, and CNFL started to significantly decrease, as early as grade 1 DED (1.446 ± 0.013, 1.483 ± 0.011, 21.129 ± 0.896 mm/mm^2, respectively) compared with the control group (1.499 ± 0.006, 1.528 ± 0.005, and 25.183 ± 0.496 mm/mm^2, respectively, $P < 0.05$), and the CNTor increased in grade 1 DED (3.307 ± 0.064 vs. 3.069 ± 0.026, $P < 0.05$). The CND_f and CNFL were further reduced in grade 3 DED (1.407 ± 0.012 and 18.720 ± 0.684 mm/mm^2) compared with grade 1 (1.446 ± 0.013 and 21.129 ± 0.896 mm/mm^2, $P < 0.05$). There was no significant difference for CNBP in grade 1 DED compared with the control ($P > 0.05$), but a significant decrease was observed in grades 2 and 3 ($P < 0.05$). The representative whorl-like nerve images before and after segmentation with specific corneal nerve geometric parameters in each group are shown in Figure 2. By contrast, geometric parameters of the straight nerve did not change significantly in grade 1 DED compared with the control group ($P > 0.05$), as detailed in Figure 3 and Table 3. In grades 2 and 3 DED, the CND_f, CND_0, CNBP, and CNFL decreased significantly compared with both grade 1 DED and the control group ($P < 0.05$), whereas the CNTor increased ($P < 0.05$).

Table 4 presents the nerve parameters for different DED subtypes. Compared with the evaporative DED group, the aqueous-deficient group demonstrated reduced CNFL (20.937 ± 0.533 vs. 18.795 ± 0.491 mm/mm^2, $P < 0.05$), CND_f (1.447 ± 0.008 vs. 1.408 ± 0.010, $P < 0.05$), CND_0 (1.483 ± 0.007 vs. 1.452 ± 0.009, $P < 0.05$), and CNBP (310.151 ± 14.535 vs. 258.750 ± 10.126 n/mm^2, $P < 0.05$) at the whorl region, and reduced CNFL (18.835 ± 0.568 vs. 17.224 ± 0.528 mm/mm^2, $P < 0.05$), CND_f (1.401 ± 0.009 vs. 1.374 ± 0.009, $P < 0.05$) and CND_0 (1.437 ± 0.008 vs. 1.411 ± 0.007, $P < 0.05$) for the straight nerve. The CNTor of the straight nerve was increased in the aqueous-deficient DED group compared with the evaporative DED group (3.227 ± 0.035 vs. 3.361 ± 0.037, $P < 0.05$).

Evaluation of the Clinical Associations and Diagnostic Performance of Subbasal Nerve Plexus Parameters

The relationships between clinical characteristics of DED and whorl-like nerve parameters are summarized in Table 5. After adjustments for age and gender via GEE, the CNFL, CND_f, CND_0, and CNBP showed a negative correlation with OSDI and CFS, and CNTor was positively correlated

Table 1. Demographics and Ocular Surface Parameters for the Control and DED Groups

Characteristics	Control	DED	*P* Value
Number of eyes	51	95	
Number of subjects	29	62	
Age (yrs)	34.66 ± 11.28	39.47 ± 12.57	0.082
Sex distribution (female/male)	14/15	42/20	0.075
OSDI score	3.89 ± 2.84	32.27 ± 15.92	<0.001
Clinical data			
TBUT (sec)	14.44 ± 5.07	5.49 ± 4.61	<0.001
CFS	0	2.88 ± 2.77	<0.001
Schirmer I test (mm)	17.39 ± 8.08	11.62 ± 9.87	0.002
Central corneal sensitivity (cm)	5.78 ± 0.34	5.79 ± 0.40	0.726
Periphery cornea sensitivity (cm)	5.63 ± 0.47	5.68 ± 0.47	0.538
Dry eye severity		Grade 1: 15 (16%) Grade 2: 52 (55%) Grade 3: 28 (29%)	
Dry eye subtype		Evaporative: 55 (58%) Aqueous-deficient: 40 (42%)	

Data are presented as mean ± standard deviation; the chi-square test was used to compare groups by gender; The Mann−Whitney *U* test was used to compared ocular surface parameters between groups; *P* values in bold indicate statistically significant differences. CFS = corneal fluorescein staining; DED = dry eye disease; OSDI = ocular surface disease index; TBUT = tear film break-up time.

with them ($P < 0.01$). The CNFL, CND_f, CND_0, and CNBP were positively correlated with TBUT ($P < 0.05$), whereas it was negatively correlated with CNTor. The CNFL, CND_f, and CND_0 were positively associated with Schirmer I ($P < 0.01$). However, there was no association between nerve metrics and corneal sensation ($P > 0.05$).

Of 10 corneal nerve parameters collected from participants, 4 parameters were selected based on nonzero coefficients calculated by least absolute shrinkage and selection operator regression analysis (Fig 4). These parameters included whorl-like CNFL, whorl-like CNTor, linear CND_f, and linear CNTor. To generate a predictive model for DED, multivariable logistic regression analysis was conducted based on the above 4 parameters selected by the least absolute shrinkage and selection operator regression model (Fig 5). The AUC for the proposed model was 0.910 (95% confidence interval, 0.861−0.949) after bootstrapping (resampling = 1000) for internal validation (Fig 5). The Hosmer−Lemeshow test yielded a *P* value of 0.813, indicating that the model was well-calibrated (Fig 5).

Discussion

Traditional morphological analysis of corneal nerves has primarily focused on the straight structure at the central cornea.[11,12,15,16,40] However, because of the limited field of view of IVCM, it is challenging to objectively evaluate the overall changes of corneal nerves. Previous studies have suggested that the whorl region offers an ideal position to assess corneal nerve.[19,20,41] Nevertheless, the complex curvilinear nature of whorl-like nerves requires higher segmentation accuracy and a broader range of parameters to capture their distinctive characteristics. In this article, we used artificial intelligence-based segmentation algorithm and methods to quantify the whorl-like nerve and demonstrated its geometric parameters were significant indicators for severity of DED. Moreover, significant nerve fiber loss was found at the whorl-like region in the aqueous-deficient DED compared with the evaporative DED. In addition, geometric parameters based on IVCM images of corneal nerves showed good performance in diagnosing DED.

Table 2. Clinical Findings in Different DED Severity Based on DEWS Classification

	DEWS Clinical Severity in DED Group			
Ocular Surface Parameters	*Grade 1 (n = 15)*	*Grade 2 (n = 52)*	*Grade 3 (n = 28)*	**P Value (GEE)**
OSDI score	20.14 ± 7.32	29.80 ± 14.71*	44.04 ± 15.79*,†	<0.001
TBUT (sec)	8.73 ± 3.52	5.30 ± 4.87*	4.12 ± 3.90*	<0.001
CFS	0.87 ± 1.46	2.21 ± 2.33*	4.86 ± 2.72*,†	<0.001
Schirmer I test (mm)	18.53 ± 9.46	14.00 ± 10.04	4.50 ± 4.84*,†	<0.001

Data are presented as mean ± standard deviation. CFS = corneal fluorescein staining; DED = dry eye disease; DEWS = Dry Eye Workshop; OSDI = ocular surface disease index; TBUT = tear film break-up time.
*$P < 0.05$ compared with grade 1.
†$P < 0.05$ compared with grade 2 assessed by general estimating equation.

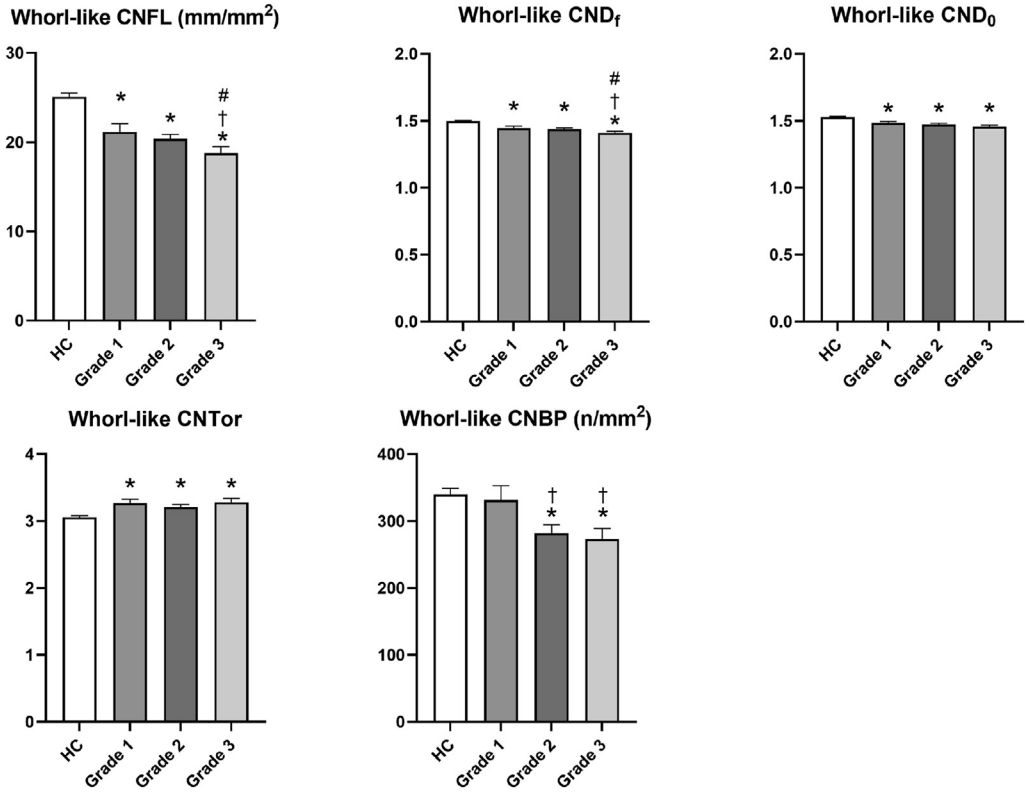

Figure 1. Changes in geometric parameters of the whorl region across different DED severities. *Compared with the healthy controls, $P < 0.05$; †Compared with grade 1 DED, $P < 0.05$; #Compared with grade 2 DED, $P < 0.05$; P value was based on GEE analysis accounting for the correlation between eyes of the same participant with gender and age as a covariate. CNBP = corneal nerve branching point; CND_f = corneal nerve fractal dimension; CND_0 = corneal nerve multifractal dimension; CNFL = corneal nerve fiber length; CNTor = corneal nerve tortuosity; DED = dry eye disease; GEE = generalized estimating equation; HC = healthy control.

Although noninvasive IVCM could provide high-resolution in vivo images of microstructure for dry eye evaluations, including nerves and inflammatory cells, lack of scoring systems and quantitative methods is one of the major problems hindering its wide application.[42] Interestingly, our findings revealed that changes in CND_f,

Table 3. In Vivo Confocal Microscopic Findings in Different Severities of DED Based on DEWS Classification

		DEWS Clinical Severity in DED Group		
Corneal Nerve Parameters	**Control (n = 51)**	*Grade 1 (n = 15)*	*Grade 2 (n = 52)*	*Grade 3 (n = 28)*
Whorl-like nerve				
CNFL (mm/mm²)	25.183 ± 0.496	21.129 ± 0.896*	20.434 ± 0.533*	18.720 ± 0.684*,†,‡
CND_f (unitless)	1.499 ± 0.006	1.446 ± 0.013*	1.440 ± 0.010*	1.407 ± 0.012*,†,‡
CND_0 (unitless)	1.528 ± 0.005	1.483 ± 0.011*	1.474 ± 0.008*	1.456 ± 0.010*
CNBP (n/mm²)	364.092 ± 11.706	337.162 ± 18.927	284.720 ± 12.263*,†	270.750 ± 15.910*,†
CNTor (unitless)	3.069 ± 0.026	3.307 ± 0.064*	3.221 ± 0.040*	3.289 ± 0.059*
Straight nerve				
CNFL (mm/mm²)	21.431 ± 0.321	22.043 ± 0.808	17.203 ± 0.452*,†	17.912 ± 0.477*,†
CND_f (unitless)	1.449 ± 0.006	1.456 ± 0.011	1.372 ± 0.007*,†	1.388 ± 0.008*,†
CND_0 (unitless)	1.473 ± 0.006	1.487 ± 0.009	1.412 ± 0.006*,†	1.423 ± 0.008*,†
CNBP (n/mm²)	227.759 ± 8.629	262.291 ± 15.647	144.429 ± 7.535*,†	187.020 ± 15.448*,†
CNTor (unitless)	3.093 ± 0.035	3.087 ± 0.039	3.337 ± 0.034*,†	3.289 ± 0.042*,†

Data presented as mean ± standard error. CNBP = corneal nerve branching point; CND_f = corneal nerve fractal dimension; CND_0 = corneal nerve multifractal dimension; CNFL = corneal nerve fiber length; CNTor = corneal nerve tortuosity; DED = dry eye disease; DEWD = Dry Eye Workshop.
*$P < 0.05$ compared with controls.
†$P < 0.05$ compared with grade 1.
‡$P < 0.05$ compared with grade 2.

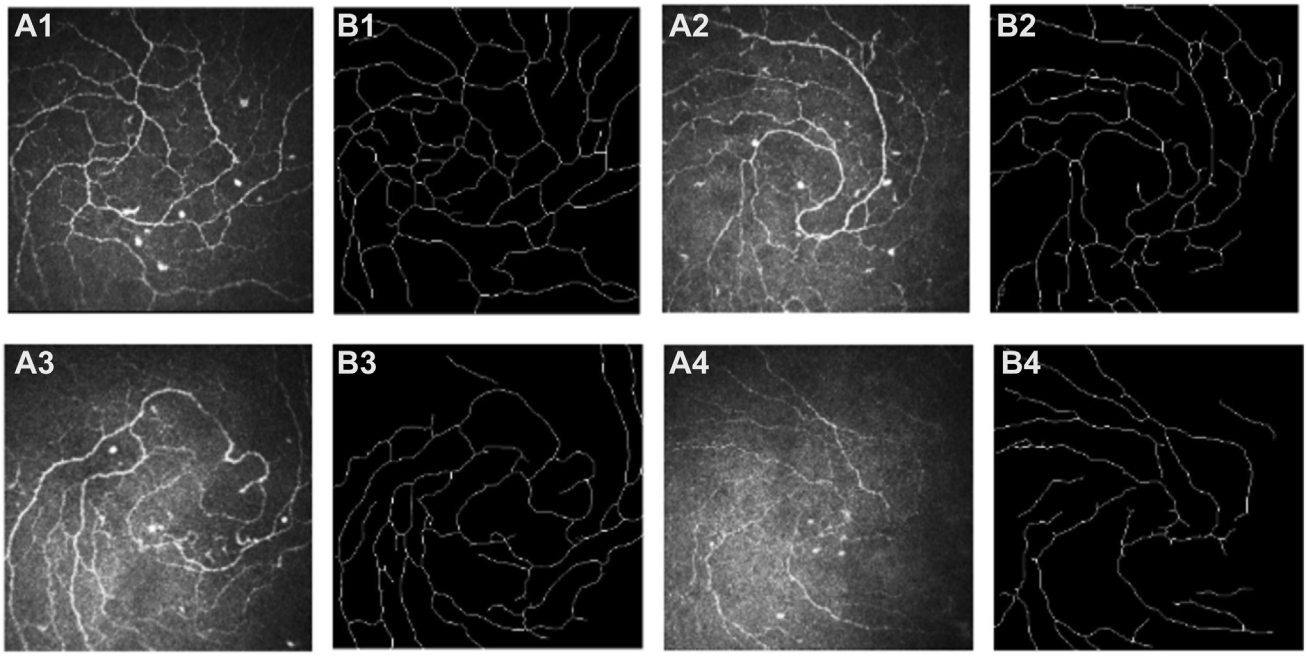

Figure 2. In vivo confocal microscopy images of whorl-like corneal nerve across different DED severities. Original corneal image (**A**) and corresponding skeletonized map (**B**); The order from 1 to 4 was: normal subjects, grade 1, grade 2, and grade 3 DED patients. DED = dry eye disease.

corneal CND_0, CNFL, and CNTor were easily detected in the IW region in the mild DED, whereas there were no changes in the straight structure compared with the control group. Furthermore, most studies based on IVCM have reported reduced density and increased tortuosity for corneal straight nerve in DED patients compared with normal controls, even though the changing trend across different DED severity has not been describe.[11,43–45] Our results suggested that CND_f, CND_0, and CNFL in IW region decreased in grade 1 DED and further decreased in grade 3. The CNTor increased in each grade compared with the control group. These results suggested morphological parameters of IW were significant indicators for severity of DED.

The geometric alterations of corneal nerve were closely linked with pathophysiological mechanism of DED. It has been well documented that corneal nerve injury is linked with ocular surface inflammation.[46] Moreover, when the tear film covering the eye surface becomes thin, the mechanical stress induced by blinking is abnormally increased,[47] resulting in peripheral corneal nerve damage.[48] This injury initiates a cycle of degeneration and regeneration of nerves, resulting in structural changes in corneal nerve fibers, which exhibit reduced density, length, and increased tortuosity.[14] In addition, neurometabolic alterations induced by tissue damage and released nerve growth factors also contributed to the increased tortuosity.[49] Interestingly, previous studies showed that a decrease in length of whorl-like nerve rather than linear nerve length was detected in diabetic patients without polyneuropathy,[21,50] and similar results were obtained in studies regarding neurological diseases.[20,51] It is presumed that corneal nerve degradation may firstly occur in a more distal and highly innervated region, the IW. Thus, through the objective quantitative analysis of whorl-like nerve morphology, it is likely to establish a precision diagnosis and therapy system for DED.

The present study also investigated the associations between geometric parameters of whorl-like cornea nerve and ocular manifestations related to neurological function. The findings revealed that the Schirmer I test had a positive correlation with CND_f and CNFL. Likewise, evident nerve fiber loss was found at the whorl-like region for aqueous-deficient DED in our study. According to Cox et al,[16] more pronounced loss of corneal subbasal nerves was observed in aqueous-deficient DED compared with evaporative DED. It is therefore presumed that degeneration of corneal nerve networks is probably implicated in reduced tear production, through disrupting the tear secretion pathway. However, it is also possible that aqueous deficiency itself can cause elevated inflammation and subsequent nerve loss.[52]

In addition, previous studies have confirmed that nerves play an important role in maintaining corneal epithelial homeostasis. Kheirkhah et al,[53] in their randomized clinical trial, showed that significant improvement in corneal staining score were observed only in DED group with near-normal CNFL after treatment, which underlined the trophic support of corneal nerves. Previous case–control studies have also demonstrated density or length of corneal nerves was negatively correlated with corneal staining score, which is consistent with our results.[11,40] As we know, because there is fair amount of redundancy in corneal nerves, the semiquantitative Cochet–Bonnet

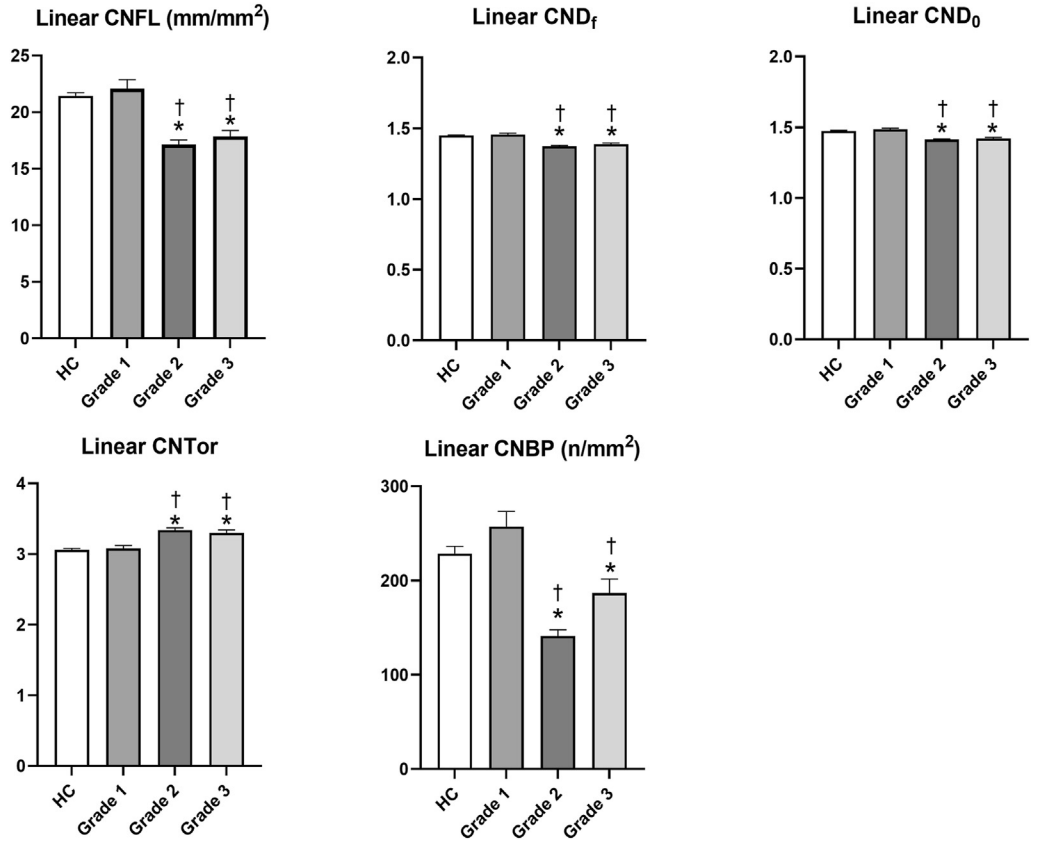

Figure 3. Changes in geometric parameters of the linear nerve across different DED severities. *Compared with the healthy controls, $P < 0.05$; †Compared with grade 1 DED, $P < 0.05$; *P* value was based on GEE analysis accounting for the correlation between eyes of the same participant with gender and age as a covariate. CNBP = corneal nerve branching point; CND_f = corneal nerve fractal dimension; CND_0 = corneal nerve multifractal dimension; CNFL = corneal nerve fiber length; CNTor = corneal nerve tortuosity; DED = dry eye disease; GEE = generalized estimating equation; HC = healthy control.

aesthesiometer may not be able to detect changes in corneal sensitivity caused by subtle changes in nerve morphology.[54] Therefore, it is reasonable that nerve morphology is not associated with corneal sensitivity in our current study. The OSDI includes items regarding pain, and sensitivity to light and windy conditions, which may reflect neurologic

Table 4. In Vivo Confocal Microscopic Findings in Different Subtypes of DED

Corneal Nerve Parameters	Control (n = 51)	Evaporative DED (n = 55)	Aqueous-Deficient DED (n = 40)
Whorl-like nerve			
CNFL (mm/mm²)	25.173 ± 0.496	20.937 ± 0.533*	18.795 ± 0.491*,†
CND_f (unitless)	1.499 ± 0.006	1.447 ± 0.008*	1.408 ± 0.010*,†
CND_0 (unitless)	1.528 ± 0.005	1.483 ± 0.007*	1.452 ± 0.009*,†
CNBP (n/mm²)	364.057 ± 11.576	310.151 ± 14.535*	258.750 ± 10.126*,†
CNTor (unitless)	3.068 ± 0.025	3.218 ± 0.033*	3.288 ± 0.061*
Straight nerve			
CNFL (mm/mm²)	21.449 ± 0.333	18.835 ± 0.568*	17.224 ± 0.528*,†
CND_f (unitless)	1.449 ± 0.006	1.401 ± 0.009*	1.374 ± 0.009*,†
CND_0 (unitless)	1.473 ± 0.006	1.437 ± 0.008*	1.411 ± 0.007*,†
CNBP (n/mm²)	228.313 ± 9.056	184.291 ± 11.882*	161.804 ± 12.440*
CNTor (unitless)	3.091 ± 0.036	3.227 ± 0.035*	3.361 ± 0.037*,†

Data presented as mean ± standard error. *P* value was based on post hoc pairwise comparison testing within the generalized estimating equation analysis. CNBP = corneal nerve branching point; CND_f = corneal nerve fractal dimension; CND_0 = corneal nerve multifractal dimension; CNFL = corneal nerve fiber length; CNTor = corneal nerve tortuosity; DED = dry eye disease.
*$P < 0.05$ compared with the control group.
†$P < 0.05$ compared with the evaporative DED group.

Table 5. Association between Clinical Signs of DED and Geometrical Parameters of the Whorl-like Nerve

Outcome	OSDI	TBUT	Schirmer I	CFS	Corneal Sensation
CNFL (mm/mm^2)					
β	−1.934*	0.349*	0.442*	−0.246*	0.002
P	<0.001	0.012	0.010	<0.001	0.858
CND_f					
β	−119.2*	20.26*	32.09*	−15.97*	0.204
P	<0.001	0.027	0.003	<0.001	0.743
CND_0					
β	−115.8*	24.65*	35.68*	−17.91*	0.334
P	<0.001	0.026	0.002	<0.001	0.641
CNBP (n/mm^2)					
β	−0.055*	0.013*	0.016	−0.009*	0.001
P	0.001	0.030	0.058	<0.001	0.919
CNTor					
β	17.70*	−5.593*	−3.106	2.115*	−0.054
P	<0.001	0.015	0.360	0.022	0.703

CFS = corneal fluorescein staining; CNBP = corneal nerve branching point; CND_f = corneal nerve fractal dimension; CND_0 = corneal nerve multifractal dimension; CNFL = corneal nerve fiber length; CNTor = corneal nerve tortuosity; DED = dry eye disease; OSDI = ocular surface disease index; TBUT = tear film break-up time.
*β coefficient with $P < 0.05$.

abnormalities.[55] When corneal nerves are injured, they can develop hyperalgesia and allodynia (neuropathic pain).[56] The presence of a neuropathic activity may give rise to ongoing discomfort manifested as dryness. For eyes with DED, previous studies have also reported that lower CNFL and higher CNTor were associated with more severe OSDI.[43,57] Notably, previous studies merely correlated linear nerve morphology with ocular parameters. Thus, it is presumed that the whorl-like nerve morphology can reflect the altered ocular surface parameters as well in the DED setting.

Relatively few studies reported the performance of corneal nerve parameters in diagnosing DED, especially for the whorl region. Giannaccare et al[15] showed that corneal nerve fiber width had an AUC of 0.828 for the diagnosis of DED. However, only patients with

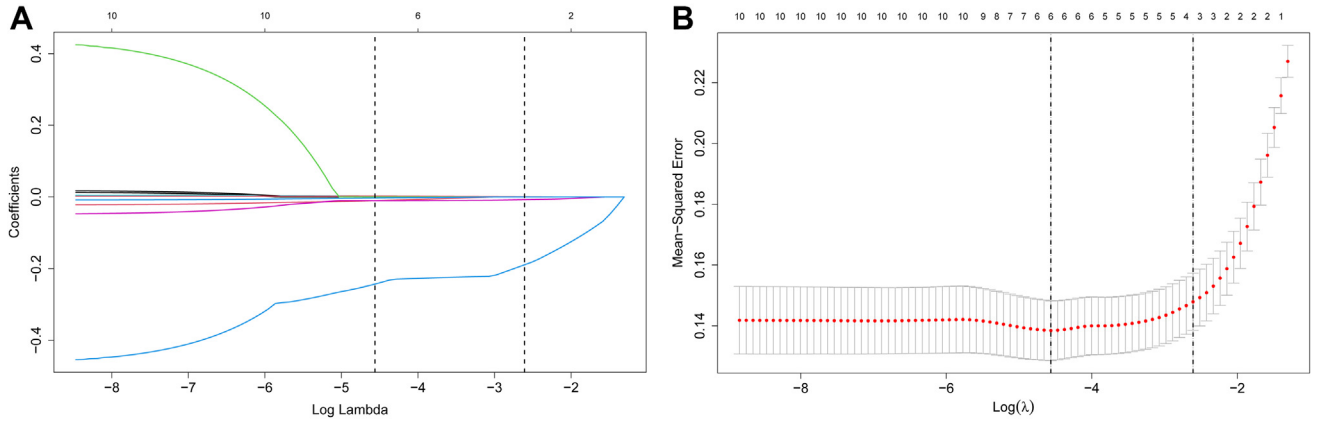

Figure 4. Selection of corneal nerve features using the LASSO regression analysis with 10-fold cross-validation. **A,** A coefficient profile plot was produced against the log(λ) sequence. This figure displays 10 variables (represented by 10 lines of different colors), where each curve depicts the trajectory of coefficient changes for an individual predictor variable. As log(λ) increases, the regression coefficients converge toward zero, ultimately resulting in a model with fewer variables. The vertical axis indicates coefficient values, and the lower horizontal axis represents log(λ), whereas the upper horizontal axis shows the number of nonzero coefficients in the model. **B,** Distribution of the mean squared error with the associated log(λ) value in the LASSO regression model. The x-axis represents log(λ), and the y-axis shows the mean squared error, where a lower value indicates a better fit of the model. The numbers atop the plot denote the number of remaining variables in the model at different λ values. The left dashed line indicates λ_min, which minimizes the error and represents the highest model fit. The right dashed line indicates λ_1-se, 1 standard error to the right of λ_min, where the model fit is still good but with fewer variables, resulting in a simpler model. Predictor selection was based on the λ_1-se criterion, where 4 nonzero coefficients (variables) were selected for the final model. LASSO = least absolute shrinkage and selection operator; min = minimum; se = standard error.

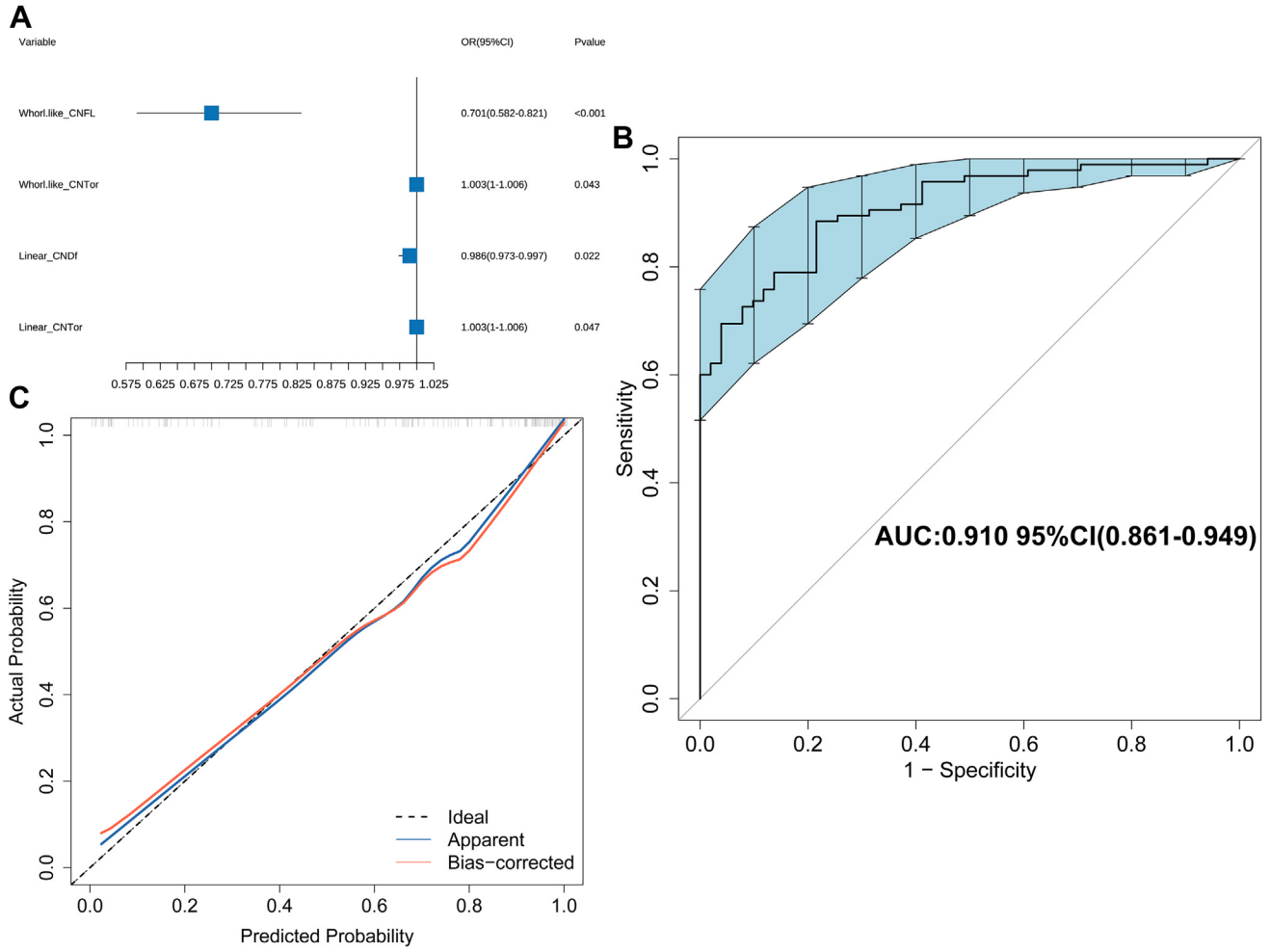

Figure 5. The diagnostic ability of subbasal nerve plexus IVCM parameters. **A,** Multivariate logistic regression used to construct the predictive model for the diagnosis of DED. **B,** Shows the AUC of internal validation using the bootstrap method (resampling = 1000). **C,** The calibration curve displayed good consistency between the actual diagnosed DED and the predicted probability (Hosmer–Lemeshow test: $P > 0.05$). AUC = area under the curve; DED = dry eye disease; IVCM = in vivo confocal microscopy.

moderate-to-severe DED affected by Sjögren syndrome or ocular graft versus host disease were included in their study. Cardigos et al[40] reported corneal nerve length had an AUC of 0.869 for discriminating Sicca syndrome from normal control subjects. However, only linear nerve images from the central cornea were selected for analysis in their study. Our study included patients with DED across different severity and the exploratory results of the diagnostic value showed an AUC of 0.91 through combining quantified nerve parameters at the whorl region and central cornea, suggesting its potential clinical application value.

Some possible limitations of this study must be considered. First, our sample size is limited, warranting additional validation studies in a larger DED population. Second, the cross-sectional study design limits causal inferences, emphasizing the need for future longitudinal treatment cohorts to confirm the relationship between corneal nerve morphology changes and DED signs. Besides, the impact of disease duration on attrition and regeneration patterns should be considered in future studies. Third, although we used rigorous internal validation, the diagnosis of DED via corneal nerve metrics in different regions is exploratory and lacks external validation; thus, large-scale studies are needed to confirm the findings.

In conclusion, this study shows that quantitative analysis of the whorl-like zone of the SBNP could provide a precise assessment of nerve alterations in varying DED severities. Moreover, the morphology parameters of the whorl-like nerve are associated with the clinical signs of DED. These findings offer novel insights for the future clinical diagnosis and treatment of DED.

Footnotes and Disclosures

Originally received: August 11, 2024.
Final revision: November 3, 2024.
Accepted: December 2, 2024.
Available online: December 5, 2024.Manuscript no. XOPS-D-24-00290R1.

State Key Laboratory of Ophthalmology, Zhongshan Ophthalmic Centre, Sun Yat-Sen University, Guangzhou, Guangdong, China.

Z.F. and K.Y. contributed equally to this work.

Disclosures:

All authors have completed and submitted the ICMJE disclosures form.

The authors have made the following disclosures:

Z.F.: Support — National Natural Science Foundation of China (Nos. 82230033 and 82271133) and Department of Science and Technology of Guangdong Province (Nos. 2021TX06Y127 and 2021TQ06Y137).

K.Y.: Support — National Natural Science Foundation of China (Nos. 82230033 and 82271133) and Department of Science and Technology of Guangdong Province (Nos. 2021TX06Y127 and 2021TQ06Y137).

Y.C.: Support — National Natural Science Foundation of China (Nos. 82230033 and 82271133) and Department of Science and Technology of Guangdong Province (Nos. 2021TX06Y127 and 2021TQ06Y137).

G.W.: Support — National Natural Science Foundation of China (Nos. 82230033 and 82271133) and Department of Science and Technology of Guangdong Province (Nos. 2021TX06Y127 and 2021TQ06Y137).

Y.D.: Support — National Natural Science Foundation of China (Nos. 82230033 and 82271133) and Department of Science and Technology of Guangdong Province (Nos. 2021TX06Y127 and 2021TQ06Y137).

W.W.: Support — National Natural Science Foundation of China (Nos. 82230033 and 82271133) and Department of Science and Technology of Guangdong Province (Nos. 2021TX06Y127 and 2021TQ06Y137).

R.X.: Support — National Natural Science Foundation of China (Nos. 82230033 and 82271133) and Department of Science and Technology of Guangdong Province (Nos. 2021TX06Y127 and 2021TQ06Y137).

Z.Y.: Support — National Natural Science Foundation of China (Nos. 82230033 and 82271133) and Department of Science and Technology of Guangdong Province (Nos. 2021TX06Y127 and 2021TQ06Y137).

P.X.: Support — National Natural Science Foundation of China (Nos. 82230033 and 82271133) and Department of Science and Technology of Guangdong Province (Nos. 2021TX06Y127 and 2021TQ06Y137).

J.Y.: Support — National Natural Science Foundation of China (Nos. 82230033 and 82271133) and Department of Science and Technology of Guangdong Province (Nos. 2021TX06Y127 and 2021TQ06Y137).

Supported by the National Natural Science Foundation of China (Nos. 82230033 and 82271133) and Department of Science and Technology of Guangdong Province (Nos. 2021TX06Y127 and 2021TQ06Y137).

HUMAN SUBJECTS: Human subjects were included in this study. This study was approved by the Medical Ethics Committee of Zhongshan Ophthalmic Center (2021KYPJ124). All research adhered to the tenets of the Declaration of Helsinki. All participants provided informed consent.

No animal subjects were included in this study.

Author Contributions:

Conception and design: Feng, Yu, Xiao, Yuan

Data collection: Feng, Yu, Deng, Xu, Zhang

Analysis and interpretation: Feng, Yu, Chen, G. Wang, W. Wang

Obtained funding: N/A

Overall responsibility: Feng, Yu

Abbreviations and Acronyms:
AUC = area under the receiver operating characteristic curve; **CFS** = corneal fluorescein staining; **CNBP** = corneal nerve branching point; **CND_f** = corneal nerve fractal dimension; **CND_0** = corneal nerve multifractal dimension; **CNFL** = corneal nerve fiber length; **CNTor** = corneal nerve tortuosity; **DED** = dry eye disease; **GEE** = generalized estimating equation; **IVCM** = in vivo confocal microscopy; **IW** = inferior whorl; **OSDI** = ocular surface disease index; **SBNP** = subbasal nerve plexus; **TBUT** = tear film break-up time.

Keywords:
Artificial intelligence, Corneal confocal microscopy, Corneal nerve, Dry eye disease.

Correspondence:
Jin Yuan, MD, PhD, 7 Jinsui Road, Tianhe District, Guangzhou, China, 510060. E-mail: yuanjincornea@126.com; and Peng Xiao, PhD, 7 Jinsui Road, Tianhe District, Guangzhou, China, 510060. E-mail: xiaopengaddis@hotmail.com.

References

1. Li M, Zeng L, Mi S, et al. A multicenter study of the prevalence of dry eye disease in Chinese refractive surgery candidates. *Ophthalmic Res*. 2021;64:224–229.
2. Liu NN, Liu L, Li J, Sun YZ. Prevalence of and risk factors for dry eye symptom in mainland china: a systematic review and meta-analysis. *J Ophthalmol*. 2014;2014:748654.
3. Yang W, Luo Y, Wu S, et al. Estimated annual economic burden of dry eye disease based on a multi-center analysis in China: a retrospective study. *Front Med (Lausanne)*. 2021;8:771352.
4. The definition and classification of dry eye disease: report of the Definition and Classification Subcommittee of the International Dry Eye WorkShop (2007). *Ocul Surf*. 2007;5:75–92.
5. Belmonte C, Nichols JJ, Cox SM, et al. TFOS DEWS II pain and sensation report. *Ocul Surf*. 2017;15:404–437.
6. Yang AY, Chow J, Liu J. Corneal innervation and sensation: the eye and beyond. *Yale J Biol Med*. 2018;91:13–21.
7. Medeiros CS, Santhiago MR. Corneal nerves anatomy, function, injury and regeneration. *Exp Eye Res*. 2020;200:108243.
8. Oliveira-Soto L, Efron N. Morphology of corneal nerves using confocal microscopy. *Cornea*. 2001;20:374–384.
9. Jalbert I, Stapleton F, Papas E, et al. In vivo confocal microscopy of the human cornea. *Br J Ophthalmol*. 2003;87:225–236.
10. Cruzat A, Qazi Y, Hamrah P. In vivo confocal microscopy of corneal nerves in health and disease. *Ocul Surf*. 2017;15:15–47.
11. Labbé A, Liang Q, Wang Z, et al. Corneal nerve structure and function in patients with non-Sjogren dry eye: clinical correlations. *Invest Ophthalmol Vis Sci*. 2013;54:5144–5150.
12. Labbé A, Alalwani H, Van Went C, et al. The relationship between subbasal nerve morphology and corneal sensation in ocular surface disease. *Invest Ophthalmol Vis Sci*. 2012;53:4926–4931.

13. Hoşal BM, Ornek N, Zilelioğlu G, Elhan AH. Morphology of corneal nerves and corneal sensation in dry eye: a preliminary study. *Eye (Lond)*. 2005;19:1276−1279.
14. Vereertbrugghen A, Galletti JG. Corneal nerves and their role in dry eye pathophysiology. *Exp Eye Res*. 2022;222:109191.
15. Giannaccare G, Pellegrini M, Sebastiani S, et al. In vivo confocal microscopy morphometric analysis of corneal subbasal nerve plexus in dry eye disease using newly developed fully automated system. *Graefes Arch Clin Exp Ophthalmol*. 2019;257:583−589.
16. Cox SM, Kheirkhah A, Aggarwal S, et al. Alterations in corneal nerves in different subtypes of dry eye disease: an in vivo confocal microscopy study. *Ocul Surf*. 2021;22: 135−142.
17. Iaccheri B, Torroni G, Cagini C, et al. Corneal confocal scanning laser microscopy in patients with dry eye disease treated with topical cyclosporine. *Eye (Lond)*. 2017;31: 788−794.
18. Badian RA, Andréasson M, Svenningsson P, et al. The pattern of the inferocentral whorl region of the corneal subbasal nerve plexus is altered with age. *Ocul Surf*. 2021;22:204−212.
19. Utsunomiya T, Nagaoka T, Hanada K, et al. Imaging of the corneal subbasal whorl-like nerve plexus: more accurate depiction of the extent of corneal nerve damage in patients with diabetes. *Invest Ophthalmol Vis Sci*. 2015;56: 5417−5423.
20. Zhang Y, Liu Z, Zhang Y, et al. Corneal sub-basal whorl-like nerve plexus: a landmark for early and follow-up evaluation in transthyretin familial amyloid polyneuropathy. *Eur J Neurol*. 2021;28:630−638.
21. Petropoulos IN, Ferdousi M, Marshall A, et al. The inferior whorl for detecting diabetic peripheral neuropathy using corneal confocal microscopy. *Invest Ophthalmol Vis Sci*. 2015;56:2498−2504.
22. Lagali N, Poletti E, Patel DV, et al. Focused tortuosity definitions based on expert clinical assessment of corneal subbasal nerves. *Invest Ophthalmol Vis Sci*. 2015;56:5102−5109.
23. Liu YC, Lin MT, Mehta JS. Analysis of corneal nerve plexus in corneal confocal microscopy images. *Neural Regen Res*. 2021;16:690−691.
24. Zhang Y, Wu Y, Li W, Huang X. Semiautomated and automated quantitative analysis of corneal sub-basal nerves in patients with DED with ocular pain using IVCM. *Front Med (Lausanne)*. 2022;9:831307.
25. Li Q, Feng B, Xie L, et al. A cross-modality learning approach for vessel segmentation in retinal images. *IEEE Trans Med Imaging*. 2016;35:109−118.
26. Wei S, Shi F, Wang Y, et al. A deep learning model for automated sub-basal corneal nerve segmentation and evaluation using in vivo confocal microscopy. *Transl Vis Sci Technol*. 2020;9:32.
27. Schiffman RM, Christianson MD, Jacobsen G, et al. Reliability and validity of the Ocular Surface Disease Index. *Arch Ophthalmol*. 2000;118:615−621.
28. Lemp MA. Report of the National Eye Institute/Industry workshop on Clinical Trials in Dry Eyes. *CLAO J*. 1995;21: 221−232.
29. Wolffsohn JS, Arita R, Chalmers R, et al. TFOS DEWS II Diagnostic Methodology report. *Ocul Surf*. 2017;15:539−574.
30. Wan Q, Wan P, Liu W, et al. Tear film cytokines as prognostic indicators for predicting early recurrent pterygium. *Exp Eye Res*. 2022;222:109140.
31. Na KS, Mok JW, Kim JY, et al. Correlations between tear cytokines, chemokines, and soluble receptors and clinical severity of dry eye disease. *Invest Ophthalmol Vis Sci*. 2012;53:5443−5450.
32. Suzuki M, Massingale ML, Ye F, et al. Tear osmolarity as a biomarker for dry eye disease severity. *Invest Ophthalmol Vis Sci*. 2010;51:4557−4561.
33. Kheirkhah A, Rahimi Darabad R, Cruzat A, et al. Corneal epithelial immune dendritic cell alterations in subtypes of dry eye disease: a pilot in vivo confocal microscopic study. *Invest Ophthalmol Vis Sci*. 2015;56:7179−7185.
34. Gong Q, Huang K, Li K, et al. Structural and functional changes of binocular corneal innervation and ocular surface function after unilateral SMILE and tPRK. *Br J Ophthalmol*. 2024;108:1492−1499.
35. Yu K, Chen Y, Feng Z, et al. Segmentation and multiparametric evaluation of corneal whorl-like nerves for in vivo confocal microscopy images in dry eye disease. *BMJ Open Ophthalmol*. 2024;9:e001861.
36. Petropoulos IN, Al-Mohammedi A, Chen X, et al. The utility of corneal nerve fractal dimension analysis in peripheral neuropathies of different etiology. *Transl Vis Sci Technol*. 2020;9:43.
37. Doubal FN, MacGillivray TJ, Patton N, et al. Fractal analysis of retinal vessels suggests that a distinct vasculopathy causes lacunar stroke. *Neurology*. 2010;74:1102−1107.
38. Khansari MM, O'Neill W, Lim J, Shahidi M. Method for quantitative assessment of retinal vessel tortuosity in optical coherence tomography angiography applied to sickle cell retinopathy. *Biomed Opt Express*. 2017;8:3796−3806.
39. Wang G, Li M, Yun Z, et al. A novel multiple subdivision-based algorithm for quantitative assessment of retinal vascular tortuosity. *Exp Biol Med (Maywood)*. 2021;246: 2222−2229.
40. Cardigos J, Barcelos F, Carvalho H, et al. Tear meniscus and corneal sub-basal nerve plexus assessment in primary Sjögren syndrome and Sicca syndrome patients. *Cornea*. 2019;38: 221−228.
41. Ferdousi M, Kalteniece A, Petropoulos I, et al. Diabetic neuropathy Is characterized by progressive corneal nerve fiber loss in the central and inferior whorl regions. *Invest Ophthalmol Vis Sci*. 2020;61:48.
42. Baudouin C, Aragona P, Van Setten G, et al. Diagnosing the severity of dry eye: a clear and practical algorithm. *Br J Ophthalmol*. 2014;98:1168−1176.
43. Ma B, Xie J, Yang T, et al. Quantification of increased corneal subbasal nerve tortuosity in dry eye disease and its correlation with clinical parameters. *Transl Vis Sci Technol*. 2021;10:26.
44. Li F, Zhang Q, Ying X, et al. Corneal nerve structure in patients with primary Sjögren's syndrome in China. *BMC Ophthalmol*. 2021;21:211.
45. Jing D, Liu Y, Chou Y, et al. Change patterns in the corneal sub-basal nerve and corneal aberrations in patients with dry eye disease: an artificial intelligence analysis. *Exp Eye Res*. 2022;215:108851.
46. Hamrah P, Seyed-Razavi Y, Yamaguchi T. Translational immunoimaging and neuroimaging demonstrate corneal neuroimmune crosstalk. *Cornea*. 2016;35(suppl 1):S20−S24.
47. Bron AJ, de Paiva CS, Chauhan SK, et al. TFOS DEWS II pathophysiology report. *Ocul Surf*. 2017;15:438−510.
48. Labetoulle M, Baudouin C, Calonge M, et al. Role of corneal nerves in ocular surface homeostasis and disease. *Acta Ophthalmol*. 2019;97:137−145.
49. Benítez-Del-Castillo JM, Acosta MC, Wassfi MA, et al. Relation between corneal innervation with confocal microscopy and corneal sensitivity with noncontact esthesiometry in

patients with dry eye. *Invest Ophthalmol Vis Sci*. 2007;48:173–181.
50. Kalteniece A, Ferdousi M, Petropoulos I, Fan D. Greater corneal nerve loss at the inferior whorl is related to the presence of diabetic neuropathy and painful diabetic neuropathy. *Sci Rep*. 2018;8:3283.
51. Jiao L, Zhang Y, Wang H, et al. Corneal confocal microscopy in the evaluation of immune-related motor neuron disease syndrome. *BMC Neurol*. 2022;22:138.
52. Patel S, Mehra D, Cabrera K, Galor A. How should corneal nerves be incorporated into the diagnosis and management of dry eye? *Curr Ophthalmol Rep*. 2021;9:65–76.
53. Kheirkhah A, Dohlman TH, Amparo F, et al. Effects of corneal nerve density on the response to treatment in dry eye disease. *Ophthalmology*. 2015;122:662–668.
54. Al-Aqaba MA, Dhillon VK, Mohammed I, et al. Corneal nerves in health and disease. *Prog Retin Eye Res*. 2019;73:100762.
55. Le DT, Kandel H, Watson SL. Evaluation of ocular neuropathic pain. *Ocul Surf*. 2023;30:213–235.
56. Guerrero-Moreno A, Baudouin C, Melik Parsadaniantz S, Réaux-Le Goazigo A. Morphological and functional changes of corneal nerves and their contribution to peripheral and central sensory abnormalities. *Front Cell Neurosci*. 2020;14:610342.
57. Tepelus TC, Chiu GB, Huang J, et al. Correlation between corneal innervation and inflammation evaluated with confocal microscopy and symptomatology in patients with dry eye syndromes: a preliminary study. *Graefes Arch Clin Exp Ophthalmol*. 2017;255:1771–1778.